J. Fluid Mech. (2001), *vol.* 442, *pp.* 359–385. Printed in the United Kingdom

Mixing in frozen and time-periodic two-dimensional vortical flows

By ALEXANDER WONHAS AND J. C. VASSILICOS†

Department of Applied Mathematics and Theoretical Physics, University of Cambridge, Silver Street, Cambridge CB3 9EW, UK

(Received 20 June 2000 and in revised form 8 February 2001)

In the first part of this paper, we investigate passive scalar or tracer advection–diffusion in frozen, two-dimensional, non-circular symmetric vortices. We develop an asymptotic description of the scalar field in a time range $1 \ll t/T \ll Pe^{1/3}$, where T is the formation time of the spiral in the vortex and Pe is a Péclet number, assumed much larger than 1. We derive the leading-order decay of the scalar variance $E(t)$ for a singular non-circular streamline geometry,

$$E(0) - E(t) \propto \left(\frac{t^3}{T^3 Pe}\right)^{\frac{2+\mu}{2}\frac{\beta}{1+\beta}}.$$

The variance decay is solely determined by a geometrical parameter μ and the exponent β describing the behaviour of the closed streamline periods. We develop a method to predict, in principle, the variance decay from snapshots of the advected scalar field by reconstructing the streamlines and their period from just two snapshots of the advected scalar field.

In the second part of the paper, we investigate variance decay in a periodically moving singular vortex. We identify three different regions (core, chaotic and KAM-tori). We find fast mixing in the chaotic region and investigate a conjecture about mixing in the KAM-tori region. The conjecture enables us to use the results from the first section and relates the Kolmogorov capacity, or box-counting dimension, of the advected scalar to the decay of the scalar variance. We check our theoretical predictions against a numerical simulation of advection–diffusion of scalar in such a flow.

1. Introduction

In this work we are interested in the influence of an advected scalar field geometry on its mixing properties. Geometrical concepts have enjoyed some popularity, both for their potential as new diagnostic tools and for their ability to improve the theoretical description of flow and mixing processes. Previous work found that the Kolmogorov capacity D_K (also known as fractal or box counting dimension, see Vassilicos & Hunt 1991) can be used to describe mixing of frozen scalar fields (Angilella & Vassilicos 1998) and mixing of a scalar field advected by a frozen, circular symmetric vortex (Flohr & Vassilicos 1997). In all these cases, when the field has a well-defined interfacial structure with a well-defined Kolmogorov capacity and when diffusion is

† Present address: Department of Aeronautics, Imperial College, Prince Consort Road, London SW7 2BY, UK.

sufficiently small and has not yet rubbed off all the scalar fine structure, the time-t-dependent scalar field variance $E(t)$ (2.15) can be described in terms of the general formula

$$E(0) - E(t) \propto \eta(t)^{D_E - D_K}, \tag{1.1}$$

where D_E is the Euclidean dimension of the embedding space and $\eta(t)$ is a dissipative micro-length scale which can depend on the flow. For example, $\eta(t) \propto \sqrt{t}$ for a static scalar field and $\eta(t) \propto \sqrt{t^3}$ for a scalar field advected by a frozen, circular symmetric vortex.

Even though (1.1) has only been derived for a limited number of cases, one may suspect that it holds true wherever interfaces are well-defined with well-defined Kolmogorov capacities D_K that are time-independent and strictly smaller than D_E. In the second part of this paper we extend the currently known domain of validity of (1.1) to scalar decay in the outer region of a periodically moving vortex. In the first part of this paper, however, we find cases where (1.1) is not valid by considering mixing in frozen two-dimensional vortical flows without circular streamlines.

Non-circular symmetric vortices are interesting to consider because two-dimensional flows, at least when strong forcing and dissipation are absent, tend to organize into isolated vortices, some of which are non-circular. Dritschel (1998) observed that an isolated patch of vorticity with a sufficiently steep edge gradient can have a stable non-axisymmetric shape and he found such non-axisymmetric vortices in simulations of inviscid two-dimensional flows. Using a numerical simulation of the Navier–Stokes equation, Rossi, Lingevitch & Bernoff (1997) showed that a strongly perturbed circular vortex can relax into a stable non-axisymmetric vortex. Le Dizès (2000) provided a theoretical analysis of non-axisymmetric vortices. Generally, they consist of a well-defined patch of vorticity. The patch itself and any passive scalar it might contain performs, to a first approximation, a solid body rotation. The velocity field outside the patch can be approximated by a frozen, non-axisymmetric flow with nested streamlines if we use Dritschel's (1998) principle of *adiabatic steadiness* and a transformation into a co-rotating frame of reference. This motivates us to investigate mixing in frozen non-axisymmetric flows which we do in § 2.

In § 3, we investigate a case of a moving vortex. Examples of moving vortices can be found in the atmosphere (one being the polar vortex), in turbulent flows and in vortical flows where vortices move subject to the influence of other vortices.

Most of this work assumes vortices with an algebraically decaying velocity field, $u \propto \rho^{-\alpha}$, where ρ indicates the distance from the centre of the vortex. Point vortices and patches of vorticity, at least in their far field, are relevant examples of such algebraic vortices with $\alpha = 1$. However, the anomalous effects of such vortices on mixing are best understood by allowing the exponent α to vary. This enables us to change the geometrical properties of the advected scalar field in measurable ways (e.g. the Kolmogorov capacity) and to identify the true nature of the geometrical influence of the scalar field. Finally, let us mention that singular algebraic vortices may be an important component of turbulent velocity fields. Hunt & Vassilicos (1991) have shown that singular vortices can be responsible for an algebraic scalar power spectrum, similar to the one predicted by Oboukhov (1949) and Corrsin (1951) for scalar mixed by a turbulent flow, and Vassilicos & Brasseur (1996) have identified such vortices in DNS of three-dimensional turbulence by use of a box-counting analysis of the vortex streamlines.

Our investigation of passive scalar advection and diffusion in two-dimensional flows has potentially a broad range of applications. First, physical realizations of two-

dimensional flows can be found. For example stably stratified flows in the stratosphere or ocean are almost planar flows, i.e. their velocity field has mainly two components. Scalar advection–diffusion in one layer of such a flow can then be approximated by a two-dimensional description. Secondly, scalar advection–diffusion is a model for the evolution of dye or passive chemical and also, to a certain extent, temperature or water vapour in such flows. Therefore this work might for example contribute to a better understanding of the formation of the ozone hole in the antarctic polar vortex, which is an isolated vortex in the stratosphere (McIntyre 1989). The chemicals involved in the formation of the ozone hole are subject to an advection–diffusion process in this vortex. Before the relevant chemical reactions can be modelled, the mixing of the chemicals has to be understood. However, the study of passive scalar advection and diffusion also offers insights into harder fluid dynamical problems. For example the advection and diffusion of vorticity, which is an active scalar in two-dimensional flows, is a very complicated nonlinear problem. Passive scalar advection and diffusion is its linear counterpart. Furthermore we hope to improve our understanding of one of the pivotal assumptions in Kolmogorov's K41 theory of turbulence. Kolmogorov assumed that the rate of decay of the kinetic energy per unit mass remains non-zero when the Reynolds number tends to infinity (see for example Frisch 1995), i.e. when the kinematic viscosity tends to zero. This translates to the problem of passive scalar variance decay being independent of molecular diffusivity κ in the limit where $\kappa \to 0$. Flohr & Vassilicos (1997) have found the limit in which scalar decay is asymptotically independent of diffusivity in certain kinds of singular vortices.

The paper is structured as follows. In § 2 we derive the leading-order decay of a scalar field in non-circular streamline geometries. For arbitrary non-circular streamlines, we show that (1.1) is not valid in general and we derive a new decay law which replaces (1.1) and which makes use of a new parameter μ, introduced here to quantify the influence of the non-circular streamline geometry. Subsection 2.4 presents a new method which allows in principle the scalar geometry to be related to its decay behaviour. Section 2 also serves as a foundation for § 3 where we drop the frozen flow condition and investigate the scalar variance decay in a periodically moving singular vortex. Two important regimes can be distinguished in space and time: a fast mixing chaotic region and a slower mixing in an outward lying KAM-tori region. Mixing in the KAM-tori region is conjectured to be similar to mixing with frozen streamlines. In § 4 we verify our theoretical predictions against a computer simulation.

2. Passive scalar advection and diffusion in frozen flows

2.1. *Orthogonal streamline coordinates*

We want to investigate the advection and diffusion of a passive scalar field $\Theta(\boldsymbol{x}, t)$ in a two-dimensional, incompressible, time-independent, vortical flow $\boldsymbol{u}(\boldsymbol{x})$. Such a flow has nested closed streamlines. It is convenient to solve the advection and advection–diffusion problems in *streamline coordinates*. A similar approach was taken by Tang & Boozer (1999), who studied the advection–diffusion equation via a global Lagrangian coordinate transformation. Global Lagrangian coordinates and our streamline coordinates can be related by a relatively simple transformation. Our streamline coordinates are denoted (ρ, φ), with $\rho \in [0; \infty]$ and $\varphi \in [0; 2\pi]$. They are chosen such that one set of coordinate lines coincides with the closed streamlines (they are the coordinate lines with $\rho = \text{const.}$) and the other set of coordinate lines are orthogonal cuts through the streamlines (they are the coordinate lines with $\varphi = \text{const.}$). Orthogonal streamline

coordinates were for example introduced by Batchelor (1956). The unit vectors of that coordinate system are given at each point $\boldsymbol{x}$ by

$$\hat{\boldsymbol{e}}_\varphi = \frac{\boldsymbol{u}(\boldsymbol{x})}{|\boldsymbol{u}(\boldsymbol{x})|}, \quad \hat{\boldsymbol{e}}_\rho = \hat{\boldsymbol{e}}_\varphi \times \hat{\boldsymbol{z}}, \tag{2.1a,b}$$

where $\hat{\boldsymbol{z}}$ is a unit vector normal to the plane. This coordinate system is defined such that the projection of the velocity $\boldsymbol{u}$ in the radial ρ-direction vanishes and therefore the only remaining component of the velocity is in the angular φ-direction

$$u_\varphi(\rho, \varphi) \equiv \boldsymbol{u} \cdot \hat{\boldsymbol{e}}_\varphi. \tag{2.2}$$

Due to vanishing u_ρ the incompressibility condition $\nabla \cdot \boldsymbol{u} = 0$ reads, in this coordinate system,

$$\frac{\partial}{\partial \varphi}[g_\rho(\rho, \varphi) u_\varphi(\rho, \varphi)] = 0. \tag{2.3}$$

The choice

$$g_\rho(\rho, \varphi) = \frac{\sqrt{\dfrac{1}{2\pi}\displaystyle\int_0^{2\pi} \mathrm{d}\varphi\, u_\varphi^2(\rho, \varphi)}}{u_\varphi(\rho, \varphi)}. \tag{2.4}$$

for the metrical component of the radial direction fulfils the incompressibility condition and proves useful in the analysis of this paper.

The metrical component g_φ of the φ-coordinate must be chosen such that the orthogonal cuts through the streamlines are indeed given by $\varphi = \text{const}$. We have the freedom of choosing g_φ on one streamline, i.e. we can parameterize one streamline in an arbitrary way. The parameterization of all other streamlines is then given by the solution of the differential equation (cf. Batchelor 1967, Appendix II)

$$\frac{\partial}{\partial \rho} g_\varphi(\rho, \varphi) = g_\rho(\rho, \varphi) \left| \frac{\partial}{\partial \varphi} \hat{\boldsymbol{e}}_\varphi(\rho, \varphi) \right|. \tag{2.5}$$

In the purely circular case, the metrical components of standard polar coordinates are given by $g_\rho|_{\text{circular}} = 1$ and $g_\varphi(\rho)|_{\text{circular}} = \rho$. We refer to coordinates as slightly non-circular if they become circular in the limit of either small or large radii, i.e. $\rho \to 0$ or $\rho \to \infty$ respectively.

2.2. *Advection–diffusion of scalar fields*

In this subsection we derive an asymptotic solution for the advection and diffusion of a scalar field in an arbitrarily nested streamline geometry. It is assumed that the average frequency of the streamlines follows the power law

$$\overline{\Omega}(\rho) \propto \rho^{-1/\beta}, \tag{2.6}$$

with $\beta > 0$. Furthermore, we assume that we are not in the pathological situation where the initial scalar interface is everywhere parallel to the streamlines. In this generic case, the flow generates a spiral interfacial structure which is independent of the initial conditions.

It is useful to write all equations in dimensionless units. A time scale T is given by the time needed to form the spiral structure. This time scale is the period of the most outward lying streamline which is touched by the initial scalar field. A length scale

L is then given by the length of the streamline with period T. All length and time scales in the rest of § 2 are non-dimensionalized with respect to these scales.†

The non-dimensionalized advection–diffusion equation for a scalar field $\Theta(\rho, \varphi, t)$ reads, in nested streamline coordinates,

$$\frac{\partial}{\partial t}\Theta(\rho, \varphi, t) + \Omega(\rho, \varphi)\frac{\partial}{\partial \varphi}\Theta(\rho, \varphi, t) = Pe^{-1}\nabla^2\Theta(\rho, \varphi, t), \tag{2.7}$$

where $Pe := L^2/(\kappa T)$ is the Péclet number, and where the angular velocity on a streamline at a point (ρ, φ) is given by

$$\Omega(\rho, \varphi) := \frac{u_\varphi(\rho, \varphi)}{g_\varphi(\rho, \varphi)}. \tag{2.8}$$

In contrast to the circular symmetric case, the angular velocity depends on the position φ on the streamline. Note that Ω must be either positive or negative for all values of ρ and φ because of the uniqueness of the advection solution in the frozen flow case. We consider in the following $\Omega > 0$ without loss of generality. Note further that $\Omega(\rho, \varphi)$ is naturally 2π-periodic in φ.

We seek a solution of (2.7) in the range of times where the flow has produced sufficient small-scale spiral structure, i.e. $t \gg 1$ in non-dimensionalized units, but has not yet completely decayed, i.e. $t \ll Pe^{1/3}$, where Pe is a sufficiently large Péclet number. Rhines & Young (1983) have already shown that the small-scale structure of the scalar field is completely diffused at times larger than $Pe^{1/3}$.

The left-hand side of (2.7), i.e. the advective contribution, can be solved by the method of characteristics, which is a transformation into an advected or Lagrangian coordinate system. Let $\varphi_0(\rho, \varphi, t)$ be the initial position of an advected tracer particle which is found at time t at position (ρ, φ). Then the solution of the pure advection equation, i.e. $Pe^{-1} = 0$, can formally be written as

$$\Theta(\rho, \varphi, t) = \Theta_{\text{ini}}(\rho, \varphi_0(\rho, \varphi, t)), \tag{2.9}$$

where Θ_{ini} is the initial scalar distribution. In Appendix A we find for the characteristic

$$\varphi_0(\rho, \varphi, t) = \varphi - \overline{\Omega}(\rho)t + \zeta(\rho, \varphi, t). \tag{2.10}$$

Hence the characteristic is given by the mean advection along the streamline, described by the averaged streamline frequency $\overline{\Omega}(\rho)$, superimposed on t- and φ-periodic oscillations, described by ζ.

We use a Fourier transformation

$$\Theta(\rho, \varphi, t) = \sum_{n=-\infty}^{\infty} \Theta_n(\rho, t)\, \mathrm{e}^{\mathrm{i}n(\varphi - \overline{\Omega}(\rho)t + \zeta(\rho, \varphi, t))} \tag{2.11}$$

to express the 2π-periodicity in the angle coordinate φ of the scalar field. Note that we consider smooth scalar fields whose Fourier coefficients decay exponentially for large enough wavenumbers. Any scalar field subject to diffusion for an infinitesimal time turns into a smooth field thereby ensuring the convergence of all Fourier series with at most algebraic pre-factors.

Carrying out an analysis of the asymptotically leading contributions to the advection–diffusion equation (2.7) in the range of times under consideration, i.e. $1 \ll t \ll Pe^{1/3}$, we find the following asymptotic solution of the advection–diffusion

† Note that these scales are different from the scales used in § 3.

equation for any nested, closed streamline geometry:

$$\Theta_n(\rho,t) = \exp\left(-\tfrac{1}{3}n^2(\bar{\Omega}'(\rho))^2\frac{t^3}{Pe}\right)\Theta_n(\rho,t=0). \tag{2.12}$$

The details of the calculation are given in Appendix B. Note that at times $t \gg Pe^{1/3}$, the scalar is smoothed out over an area covering all streamlines that have been in contact with the scalar initially, and the diffusion is much slower than in the range of times we discuss in this paper, see Rhines & Young (1983).

From (2.12) we can infer that the mixing happens faster for smaller values of ρ. The size of the inner diffused area can be found by analyzing the scaling of the argument in the exponential (2.12). The scalar on a streamline ρ is completely diffused if

$$\bar{\Omega}'(\rho)^2\frac{t^3}{Pe} \gg 1. \tag{2.13}$$

Using (2.6) it follows that the radius of the diffused core is given by

$$\rho_{\text{diff}} \propto \sqrt{\frac{t^3}{Pe}}^{\beta/(1+\beta)}. \tag{2.14}$$

This is a good measure of the extent of the region of well-mixed scalar in arbitrary closed streamline geometries. For the circular symmetric case, this result has already been derived by Flohr & Vassilicos (1997).

2.3. *Scalar variance decay in a singular vortex*

Knowing the time-evolution of Θ we can in principle calculate all scalar quantities. We are particularly interested in a description of the mixing process. One measure for mixing is the scalar variance†

$$E(t) := \int \mathrm{d}^2x\,(\Theta(\boldsymbol{x},t))^2. \tag{2.15}$$

Unlike the spatial mean of a scalar, the variance is a non-conserved quantity. It is a measure of how evenly the scalar is distributed in space and it decays during the advection–diffusion process. Its lowest value is reached when the scalar is uniformly distributed in space. The scalar variance reads, in terms of solution (2.12),

$$\begin{aligned} E(t) &= \int \mathrm{d}\rho\,\mathrm{d}\varphi\, g_\varphi(\rho,\varphi)\, g_\rho(\rho,\varphi)\,\Theta^2(\rho,\varphi,t) \\ &= \sum_{n,m}\int \mathrm{d}\rho\,\mathrm{d}\varphi\, g_\varphi(\rho,\varphi)\, g_\rho(\rho,\varphi)\exp\left(\mathrm{i}(n+m)(\varphi-\bar{\Omega}(\rho)t+\zeta(\rho,\varphi,t))\right) \\ &\quad\times\exp\left(-(n^2+m^2)(\bar{\Omega}'(\rho))^2\frac{t^3}{3Pe}\right)\Theta_n(\rho,t=0)\,\Theta_m(\rho,t=0). \end{aligned} \tag{2.16}$$

Carrying out the above integral for any given flow could be rather difficult. However if we are interested in the character of the decay in the vicinity of the flow singularity, i.e. $\rho \to 0$, we can take our analysis further.

In circular symmetric streamlines and hence without the φ-dependent terms in (2.16), the scalar variance $E(0) - E(t)$ decay is a power law in time, see Flohr &

† Normally the definition of the variance includes the subtraction of the squared mean. However, in this paper, we study quantities such as $E(0) - E(t)$, where the squared mean cancels because it is time independent.

Vassilicos (1997). We study the influence of non-circular streamlines on this power law by using a Fourier representation of the product of the metric components, i.e.

$$g_\rho(\rho,\varphi)\, g_\varphi(\rho,\varphi) = \sum_k a_k(\rho)\, \mathrm{e}^{\mathrm{i}k\varphi}. \tag{2.17}$$

Geometrically, the Fourier coefficient a_0 describes the area between two neighbouring streamlines. Hence the area between the streamlines $\rho_{\min}$ and ρ is given by

$$A(\rho) = \int_{\rho_{\min}}^{\rho} \mathrm{d}\rho' a_0(\rho'). \tag{2.18}$$

As the area in between two streamlines cannot become negative, a_0 must carry the leading behaviour in the limit $\rho \to 0$, i.e. $a_0 \geqslant a_{k\neq 0}$. We assume this leading contribution to be a power law

$$a_0(\rho) \propto \rho^{1+\mu}. \tag{2.19}$$

The parameter μ is defined such that the scaling behaviour of circular streamlines is recovered when $\mu = 0$. As $\mu \to -2$, the area between two neighbouring streamlines tends to infinity; hence $\mu > -2$. Elliptical streamline coordinates are an example of a non-trivial $\mu = -\frac{4}{3}$, see Appendix C.

Analysing the leading contribution to the variance scaling behaviour, see Appendix D, we find

$$E(0) - E(t) \propto \left(\frac{t^3}{Pe}\right)^{\frac{2+\mu}{2}\frac{\beta}{1+\beta}}. \tag{2.20}$$

This result is valid for arbitrarily nested closed streamline geometries which have a power law decay of the streamline frequency in the vicinity of their centre and in the range of times $1 \ll t \ll Pe^{1/3}$. It is assumed that the scalar field Θ itself does not possess a power law dependence on ρ. Most scalar patches with constant concentration inside their boundaries fulfil this assumption, because inside the patch the scalar concentration is non-zero and bounded from above, hence the average concentration is constant, at least on a logarithmic scale. The variance decay exponent then depends solely on the exponent μ, characterizing the geometry of the streamlines close to their centre and the exponent of the streamline frequency β.

Some insight into our result may be obtained by the following back-of-an-envelope argument. Assume that the scalar fluctuations are completely diffused at radii ρ smaller than the radius ρ_{diff} (2.14), i.e. $\Theta = \Theta_0$ for $\rho \leqslant \rho_{\mathrm{diff}}$. Assume also that scalar fluctuations have diffused at larger radii where they are characterized by Θ_{ini}. The area A of the diffused core is characterized by the radius ρ_{diff} of the diffused core and is given by $A(\rho_{\mathrm{diff}})$, see (2.14) and (2.18). Therefore the variance decay is estimated well by

$$E(0) - E(t) = \int_{\rho_{\min}}^{\rho_{\mathrm{diff}}} \mathrm{d}\rho(\Theta_{\mathrm{ini}}^2 - \Theta_0^2)\, a_0(\rho) = (\Theta_{\mathrm{ini}}^2 - \Theta_0^2)\, A(\rho_{\mathrm{diff}}), \tag{2.21}$$

which yields (2.20).

Note that the mean rate of variance decay

$$\chi = -\frac{\partial}{\partial t} E(t) \tag{2.22}$$

becomes independent of the Péclet number Pe in the case $\mu \to -2$. This means that when the area between neighbouring streamlines tends to infinity, the mean rate of variance decay becomes independent of the molecular diffusivity. Similarly, when

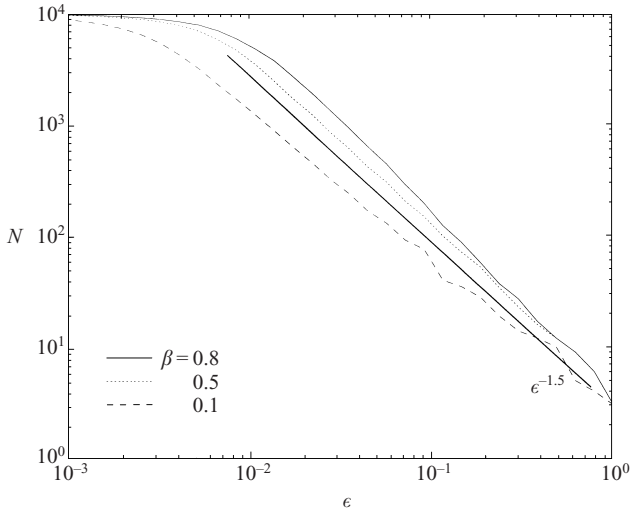

FIGURE 1. Number of square boxes N with area ϵ^2 needed to cover an elliptical spiral with $\beta = 0.8$, 0.5 and 0.1. All box-counting functions have approximately an $\epsilon^{-1.5}$ power law which implies a Kolmogorov capacity of $D_K \approx 1.5$ for all elliptical spirals irrespective of the exponent β. Note that the flattening of $N(\epsilon)$ for small values of ϵ is due to resolving the discrete points making the spiral.

$\beta \to 0$, the mean rate of variance decay becomes independent of diffusivity, too. The latter remark was made by Flohr & Vassilicos (1997) in the case of a circular symmetric vortex. They explained it in terms of the space-filling property of the spiral in the limit $\beta \to 0$.

For circular symmetric streamline geometries, μ vanishes and we recover the power law of Flohr & Vassilicos (1997). This shows in particular that in most practical situations where streamlines are near circular symmetric and μ therefore close to 0 the result of Flohr & Vassilicos (1997) holds. As in the circular symmetric case, one might assume that the decay exponent of the scalar variance decay (2.20) can be expressed in terms of the Kolmogorov capacity

$$D_K = \frac{2}{1+\beta}. \tag{2.23}$$

Flohr & Vassilicos (1997) found that the scalar variance decays in circular symmetric streamline geometries like

$$E(0) - E(t) \propto \sqrt{\frac{t^3}{Pe}}^{2-D_K}. \tag{2.24}$$

We have verified that for slightly non-circular streamlines, i.e. streamlines becoming circular in the limit of small (or large) radii, the results (2.23) and (2.24) still hold. However our numerical investigations in the case of arbitrary non-circular symmetric streamline geometry have shown that the variance decay exponent cannot be inferred from the Kolmogorov capacity D_K alone. For example in an elliptic streamline geometry with $\mu = -4/3$, the Kolmogorov capacity D_K of the advected interface is approximately 1.5 for any β ranging between 0.1 and 0.8, see figure 1. We therefore develop a new method of relating the geometrical properties of the advected scalar field to its dynamical properties in the following section.

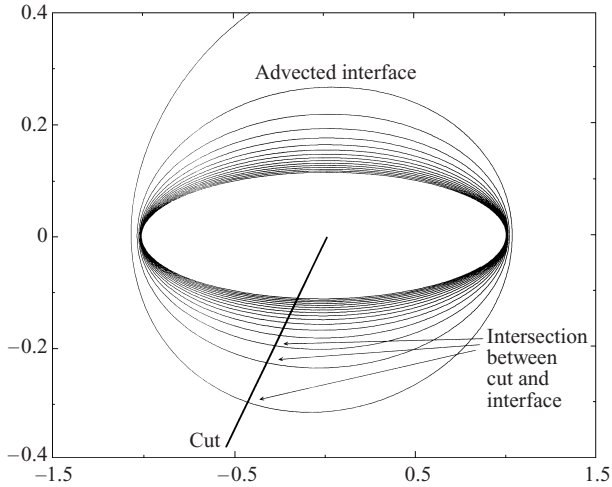

FIGURE 2. Example of a cut through an initially straight interface advected by a flow with an elliptic streamline geometry.

2.4. *Reconstruction of streamlines and their frequencies*

The aim of this subsection is to find a relation between a snapshot of the advected scalar and its variance decay in the case of arbitrary nested streamline geometries. Hence we have to develop a new method to reconstruct the streamlines and their frequencies from a snapshot of the advected scalar. The reconstructed streamlines then give the geometrical parameter μ, and the streamline frequencies determine β. This new method is based on the analysis of cuts through the advected scalar. Figure 2 shows an example of the ingredients of the method, i.e. advected interface, cut and intersection between advected interface and cut. Note that our method is applicable not only to algebraic vortices, but to any flow with nested streamlines generating a sufficient amount of scalar fine structure.

Let us consider an arbitrary nested streamline geometry. The period of a streamline with coordinate ρ is given by $T(\rho)$. We are interested in the evolution of an initially straight interface in such a flow. Note that on sufficiently small scales a smooth initial scalar distribution always has a straight interface line. The evolution of the interface in streamline coordinates is simply given by

$$\varphi(\rho) = \frac{2\pi}{T(\rho)} t + \varphi_0(\rho), \tag{2.25}$$

where the angle φ is parameterized by the radius ρ and $\varphi_0(\rho)$ describes the initial interface. This parameterization is only possible if the interface is not parallel to a streamline. However this is the case for all parts of the interface that produce some fine structure. The above relation is only strictly valid for $\varphi \bmod 2\pi = \text{const.}$, because of the possible variation of the velocity along a streamline. This condition is fulfilled in the analysis following below.

Now we consider the case where $t \gg 1$, i.e. the scalar field has developed a lot of fine structure due to the differential rotation. We assume there is an intersection between the interface and the cut at a point (ρ, φ). First, consider the cut aligned with the ρ-coordinate line, i.e. $\gamma = 0$ in figure 3. The next intersection between cut and

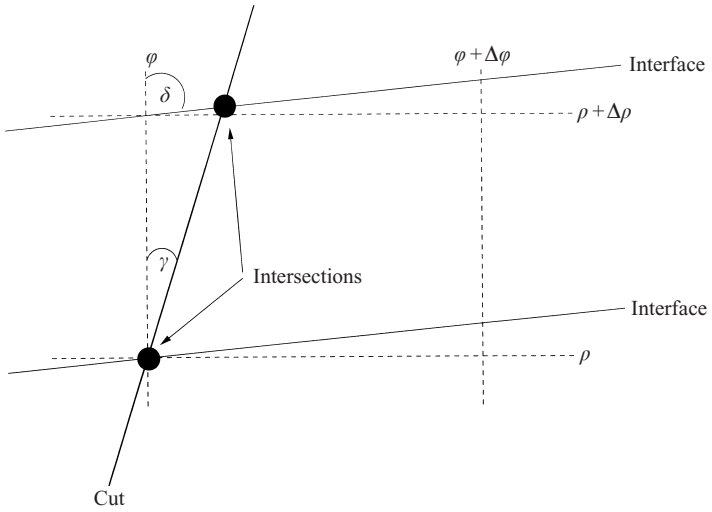

FIGURE 3. Example of a small partition of the advected interface and cut with two intersection points. The orthogonal coordinate lines are given by dashed lines, the cut and the interface are given by solid lines.

interface is then given by

$$\varphi(\rho, t) - 2\pi = \varphi(\rho + \Delta\rho, t). \tag{2.26}$$

Expanding (2.25) for small $\Delta\rho$, we find to leading order the distance between two neighbouring intersections on the cut

$$\Delta\rho = \frac{T^2(\rho)}{(\partial/\partial\rho)T(\rho)t} + O(t^{-2}), \tag{2.27}$$

for $(\partial/\partial\rho)T \neq 0$, because there must be differential shear between streamlines producing fine structure. For future use it is convenient to measure the distance between two intersections in real length s measured along the cut. As long as the cut is not parallel to a streamline, $\Delta\rho$ and $((\partial/\partial\rho)T(\rho))^{-1}$ transform identically, when ρ is replaced by the length s. The distance $\epsilon(s, t)$ between two intersections is then given by

$$\epsilon(s, t) = \frac{T^2(s)}{(\partial/\partial s)T(s)t} + O(t^{-2}). \tag{2.28}$$

This means that if there is an intersection at point s on the cut, the distance to the next intersection is given by $\epsilon(s, t)$. Note that there is no leading dependence on the initial shape of the interface.

Now consider the case where the cut has a non-zero angle γ with the ρ-coordinate line. Noting that the angle δ between the interface and the ρ-coordinate line tends to $\pi/2$ for large t, we conclude that (2.28) also holds for tilted cuts, as any variation of the cut in φ becomes irrelevant. Figure 3 is an illustration of this case.

Having established $\epsilon(s, t)$, we now reconstruct the period of the streamlines intersected by the cut. We define the time-independent part of $\epsilon(s, t)$ as

$$A(s) := \epsilon(s, t)t. \tag{2.29}$$

Generally we do not know t explicitly, but we can still calculate $A(s)$ using $\epsilon(s, t)$ at

times t and $t+\Delta t$, as Δt is known:

$$A(s) = \Delta t \frac{\epsilon(s, t+\Delta t)\,\epsilon(s,t)}{\epsilon(s,t) - \epsilon(s, t+\Delta t)}. \tag{2.30}$$

Equation (2.28) gives then an ordinary differential equation of Bernoulli type for $T(s)$, which can easily be integrated in terms of the frequency $\Omega(s) \equiv 2\pi/T(s)$:

$$\Omega(s) = -2\pi \int_{s_0}^{s} \mathrm{d}s' \frac{1}{A(s)} + \Omega(s_0). \tag{2.31}$$

Hence knowing $A(s)$ and $\Omega(s_0)$ at a certain point s_0 allows us to reconstruct the frequencies of all intersected streamlines. Note that for the purpose of calculating the streamline exponent β the constant value of $\Omega(s_0)$ is not relevant.

The task of reconstructing the full two-dimensional information about the streamlines can be performed by intersecting the nested streamline geometry with a set of cuts arranged in a star-like manner with the centre of the star at the 'centre' of the nested streamlines. Obviously, the reference point s_0 of all cuts should be identified with the centre of the star. However, if the initial scalar field vanishes in the vicinity of the centre of the star, we should use the first appearance of non-vanishing scalar along every cut as an alternative reference point because this point is very close to the most inward lying streamline that the initial non-vanishing part of the scalar field has touched. From the frequency information on each cut, we find the streamlines by interpolating between points on different cuts which have the same frequency.

We have shown that we can reconstruct the geometry and frequency of streamlines from just two snapshots taken at a known time difference, after the flow has acted for a long enough time to form a sufficient amount of fine scalar structure. Using the shape of the streamlines, we can calculate the geometrical exponent μ and using frequencies of the reconstructed streamlines, we can determine the exponent β. We are therefore able, at least in principle, to predict the decay of the scalar variance from just two snapshots of the scalar and equation (2.20).

As a final remark, we point out that the quantity $\epsilon(s,t)$ is in fact related to the Kolmogorov capacity of the scalar interface on the cut. It can even be derived from the box-counting function on the cut. The box-counting function is the number of boxes of size ϵ needed to cover the set of intersections on the cut at a given time t. Let $\Delta\epsilon$ be the change in the resolution ϵ which is necessary to go from N to $N+1$; then

$$1 \equiv N(\epsilon - \Delta\epsilon, t) - N(\epsilon, t), \tag{2.32a}$$

$$\Rightarrow \Delta\epsilon + O(\Delta\epsilon^2) = -\left(\frac{\mathrm{d}N(\epsilon,t)}{\mathrm{d}\epsilon}\right)^{-1}. \tag{2.32b}$$

Defining the position $s(\epsilon, t)$ on the cut where the distance between two intersections is ϵ, we can derive

$$s(\epsilon - \Delta\epsilon, t) = s(\epsilon, t) \mp (\epsilon - \Delta\epsilon), \tag{2.33a}$$

$$\Rightarrow \frac{\mathrm{d}s(\epsilon,t)}{\mathrm{d}\epsilon} = \pm\frac{\epsilon}{\Delta\epsilon} \mp 1 + O(\Delta\epsilon). \tag{2.33b}$$

The upper/lower sign in the $\pm$ and $\mp$ refers to the situation where the intersections come closer together for small/large values of s respectively. With (2.33*b*) we get for $\epsilon N'(\epsilon, t) \gg 1$ a relation between s and the box-counting function N on the cut:

$$\frac{\mathrm{d}s(\epsilon,t)}{\mathrm{d}\epsilon} = \mp\epsilon \frac{\mathrm{d}N(\epsilon,t)}{\mathrm{d}\epsilon}. \tag{2.34}$$

By a simple inverse operation we find $\epsilon(s,t)$ from $s(\epsilon,t)$. Recall that the Kolmogorov capacity is given by the negative exponent of ϵ in the box-counting function $N(\epsilon,t)$. Hence the connection between $\epsilon(s,t)$ and the Kolmogorov capacity of the intersections on a cut is established.

3. Passive scalar in periodically moving singular vortices

3.1. *Definition of the periodically moving singular vortex*

The periodically moving singular vortex was first considered by Aref (1984) and is described by an incompressible velocity field $\boldsymbol{u}(\boldsymbol{x},t)$. This velocity field is constructed from the frozen algebraic vortex

$$u_\phi = \Gamma r^{-\alpha}, \tag{3.1}$$

in polar coordinates (r,ϕ), by moving it as a whole with periodic displacement $\xi\,\mathrm{d}(t)$. ξ is the amplitude of the periodic displacement and $\mathrm{d}(t) = \mathrm{d}(t+T)$ is a normalized ($|\mathrm{d}(t)| \leqslant 1$) T-periodic movement. We define the frequency ω of the periodic displacement by $\omega := 2\pi/T$. Note that (3.1) is a special case of (2.6) corresponding to circular streamlines and $\beta = 1/(1+\alpha)$.

In order to establish the number of independent parameters of the flow, we revert to dimensionless variables. The natural time scale in this problem is the period T of the displacement. With the dimensional parameter $[\Gamma] = L^{1+\alpha}/T$, we can define a length scale $L := \left(\Gamma/\omega\right)^{\beta}$. This length scale is the radius of the circular streamline of the frozen vortex where an infinitesimal tracer particle is advected around the full circle of the streamline in time T. Choosing the coordinate system such that the movement happens along the x-axis, the velocity field $\boldsymbol{u}(\boldsymbol{x},t)$ reads, in dimensionless† Cartesian coordinates,

$$\boldsymbol{u}(\boldsymbol{x},t) = 2\pi\sqrt{(x-\xi\,\mathrm{d}(t))^2+y^2}^{\,-\alpha-1}\begin{pmatrix} -y \\ x-\xi\,\mathrm{d}(t)\end{pmatrix}. \tag{3.2}$$

The sole parameter of the problem is the amplitude ξ. For $\xi = 0$ we recover the frozen algebraic vortex (3.1). Hence we regard ξ as the perturbation parameter in our problem.

An example of such a periodically moving singular vortex was investigated by Vassilicos & Fung (1995) using $\mathrm{d}(t) = \sin(\omega t)$. They studied the Kolmogorov capacity of an advected interface line in such a vortex as a function of the amplitude ξ of the periodic displacement.

Note that in real flows, point vortices and patches of vorticity have an algebraically decaying velocity field for large distances from their centre. However for point vortices in viscous flows, viscosity introduces an inner cut-off of the velocity field near its centre, turning the singularity into a near-singularity. The following analysis is therefore valid for near-singular flows and patches of vorticity where the amplitude ξ of the displacement is much larger than the radius below which the velocity field loses its algebraic behaviour.

3.2. *Different regions in the periodically moving singular vortex*

In this subsection we analyse the different flow regions in the periodically moving singular vortex for small amplitudes ξ. We make intensive use of methods developed

† Note that the scales T and L used here to non-dimensionalize the flow are different from those used in § 2.

for Hamiltonian dynamical systems. For a review with emphasis on fluid dynamical problems see for example Ottino (1989).

The three-dimensional phase space is spanned by $(x, y, t \bmod 1)$ and has $1\frac{1}{2}$ degrees of freedom. The flow can be analysed by means of the Poincaré maps, or simply maps, of the flow. The Poincaré maps are defined by

$$\boldsymbol{P}_{\pm} : \boldsymbol{x}(t) \to \boldsymbol{x}(t \pm 1), \tag{3.3}$$

where $\boldsymbol{x}(t)$ is the solution of the advection equation

$$\frac{\partial}{\partial t}\boldsymbol{x}(s,t) = \boldsymbol{u}(\boldsymbol{x}(s,t)). \tag{3.4}$$

The Poincaré maps give the positions of flow-advected infinitesimal tracer particles at discrete time steps. We study one arbitrarily chosen map, because the qualitative properties of all such maps are identical.

Before investigating the influence of small perturbations ξ, let us first discuss the map in the unperturbed case $\xi = 0$. In this case, because there is no time-dependence, all Poincaré maps collapse onto one map which has the analytic expression

$$\boldsymbol{P}_{\pm} : \begin{pmatrix} r \\ \phi \end{pmatrix} \to \begin{pmatrix} r \\ \phi \pm 2\pi\, r^{-\alpha-1} \end{pmatrix}. \tag{3.5}$$

This map has an elliptic fixed point at the origin. Furthermore, the entire (x, y)-plane is partitioned into rational and irrational invariant tori. Throughout this article, tori refer to two-dimensional cuts of three-dimensional invariant tori. The rational tori are at radii

$$r_{n,m} = \left(\frac{n}{m}\right)^{-1/(1+\alpha)}, \tag{3.6}$$

where n, m are positive integers. The irrational tori occupy the rest of the plane.

Now we consider small non-vanishing perturbations ξ, i.e. $0 < \xi \ll 1$. The Taylor expansion of the velocity field (3.2) reads

$$\begin{aligned} \boldsymbol{u}(x,y,t) = {} & \underbrace{2\pi(x^2+y^2)^{-(\alpha+1)/2}\begin{pmatrix} -y \\ x \end{pmatrix}}_{\boldsymbol{u}^{(0)}} \\ & + \underbrace{\xi\, 2\pi\, \mathrm{d}(t)(x^2+y^2)^{-(\alpha+3)/2}\begin{pmatrix} -(\alpha+1)xy \\ \alpha x^2 - y^2 \end{pmatrix}}_{\boldsymbol{u}^{(1)}} + O(\xi^2). \end{aligned} \tag{3.7}$$

This expansion is a good approximation of the velocity field where the ratio of the modulus of the first-order velocity vector to the modulus of the zeroth-order velocity vector is small, i.e. $|u^{(1)}|/|u^{(0)}| \ll 1$. This condition is fulfilled where

$$\xi \ll \begin{cases} r: & 0 < \alpha < 1 \\ r/\alpha: & 1 \leqslant \alpha. \end{cases} \tag{3.8}$$

The region where the above relation does not hold is referred to as the *core region*. Outside the core region the velocity field is given by an integrable velocity field $\boldsymbol{u}^{(0)}$ plus a small non-integrable perturbation. Hence, for suitably differentiable displacements, we can apply the theorems derived for near-integrable Hamiltonian systems. On the basis of the KAM-theorem (see for example Arnold 1988), we can say that most irrational tori remain invariant tori. However their circular shape gets slightly

distorted. In contrast, the Poincaré–Birkhoff theorem (Birkhoff 1935) states that the rational tori change character and turn into sets of elliptic and hyperbolic fixed points, connected by stable and unstable manifolds. Chaotic advection occurs in these regions. The KAM-tori and the chaotic orbits are interwoven; between any two irrational tori we find infinitely many rational tori and vice versa.

It is therefore useful to establish an upper bound to the space occupied by chaotic orbits. Solving the advection equation (3.4) with a perturbation ansatz $\boldsymbol{x}(t) = \boldsymbol{x}^{(0)}(t) + \xi \boldsymbol{x}^{(1)}(t) + O(\xi^2)$ yields for the radial component of an advected tracer particle which was initially at (r_0, ϕ_0)

$$r(t) = r_0 - \xi r_0^{-\alpha-1} \int_0^t \mathrm{d}t' \, \mathrm{d}(t') \sin(\phi_0 + r_0^{-\alpha-1} t') + O(\xi^2). \tag{3.9}$$

For a KAM-torus of the unperturbed system $\boldsymbol{u}^{(0)}$, $r_0^{-\alpha-1}$ is irrational and $\sin(\phi_0 + r_0^{-\alpha-1} t')$ can therefore not resonate with $\mathrm{d}(t)$, hence the perturbation integral is of order 1. This means that the maximal deviation of the KAM-tori from the circular shape decays like $r^{-\alpha-1}$. As the chaotic orbits cannot penetrate the KAM-tori, we find a rough upper bound for the size of the chaotic regions to be the maximal distance between two neighbouring KAM-tori, which is of order $r^{-\alpha-1}$. Therefore the space occupied by chaotic orbits must at least decay like $r^{-\alpha-1}$. Hence we expect a large *chaotic region* (where the period-1 fixed points of the map turn into one hyperbolic and one elliptic fixed point and hence form a homoclinic tangle) at $r \approx 1$, because then the perturbation of the KAM-tori is of $O(1)$. For $r \gg 1$ the chaotic orbits are confined to very small areas. Consequently the scalar advection for $r \gg 1$ is governed by the KAM-tori and we refer to it as *KAM-tori region*. The numerical results of § 4 are in agreement with these predictions.

3.3. *Diffusion of scalar*

In this subsection we consider the diffusion of passive scalar in the three different regions of the vortex and make theoretical predictions which we assess numerically in § 4.

3.3.1. *Core region*

In the core region of the vortex, the time an infinitesimal tracer particle takes to travel around the centre of the vortex once is very small. Furthermore the velocity fluctuations are large. We expect therefore very fast mixing of the scalar in this region; indeed faster than in any region further out from the centre.

3.3.2. *Chaotic region*

Scalar variance decay in chaotic flows has been the subject of recent investigations by Pierrehumbert (1994), Toussaint, Carrière & Raynal (1995) and Antonsen *et al.* (1996). It was shown that the scalar variance decays exponentially in a chaotically advecting flow in the range of times we consider here. We have performed a simulation of the scalar variance decay in the chaotic region, which we report in § 4.2, and have indeed found a decay that is faster than in the same region with respect to the centre of a non-moving vortex.

3.3.3. *KAM-tori region*

Based on a Lagrangian analysis of the advection–diffusion equation, Tang & Boozer (1999) conjectured that advection–diffusion on KAM-tori is similar to advection–diffusion in an integrable flow, i.e. frozen streamlines. Hence we approximate the

time-periodic problem with a frozen streamline field in the KAM-tori-dominated region. This frozen velocity field is chosen such that the Poincaré map of the frozen flow leaves the KAM-tori of one Poincaré map of the time-periodic flow in the KAM-tori region invariant. Hence the streamlines of the frozen velocity field are identified with the KAM-tori of the time-periodic case. The period of each streamline is given by the average time needed for a tracer particle to travel around the corresponding KAM-torus once. The average period of a KAM-torus can be measured by following the trajectory of a tracer particle which belongs to the KAM-torus: the average time between two consecutive intersections of the trajectory with a radial line then defines the average period. The small chaotic regions in between the KAM-tori are neglected and replaced by appropriately chosen closed streamlines approximating the closest KAM-tori. This transformation from the time-periodic case to a frozen streamline geometry will be called *freezer transformation* in the remainder of this paper.

The transformation contains two rather bold approximations. First, the chaotic regions within the KAM-tori region are neglected. On the one hand we assume this to be a good approximation, because the size of the chaotic regions, which is bounded by (3.9), rapidly declines with distance from the centre. On the other hand, however, the chaotic regions might affect the qualitative character of mixing between KAM-tori and could hence have an impact on the decay rate of the global scalar variance. In order to support this approximation, we numerically search for fast mixing regions which would be a signature of chaotic mixing in between KAM-tori in § 4.1. At least within the limitations of our numerical resolution, we do not find any such signatures.

The second approximation lies in the fact that the trajectory of a particle in a certain KAM-torus is generally different in the time-periodic case from the trajectory of particles in the frozen flow. However, the rationale for this second approximation is that the deviations are small and progressively smaller the further away we are from the centre, see (3.9). Furthermore, the analysis of the scalar advection and diffusion in the frozen case showed that the actual shapes of slightly non-circular closed streamlines do not have a leading-order influence on the scalar variance decay. We therefore believe the approximations involved in the freezer transformation to be good approximations in the KAM-tori region.

The freezer transformation allows us to apply the results from § 2. Assuming the freezer transformation to be a good approximation, the scalar advection in the KAM-tori region may be modelled by scalar advection in a slightly non-circular frozen streamline geometry. Therefore we expect the Kolmogorov capacity D_K of the scalar advected in the KAM-tori region to be given by (2.23) with the exponent $\beta = 1/(1+\alpha)$ and α from (3.2). We have performed a box-counting analysis of the advected scalar field, as for example shown in figure 4, and found indeed the expected relation between the Kolmogorov capacity and α. Secondly, we expect the decay of the scalar variance to be given by (2.24). Hence by measuring the Kolmogorov capacity from a snapshot of the advected scalar in the KAM-tori region, we are able to predict how the scalar variance decays. In order to support the validity of the freezer transformation, we investigate numerically the scalar variance decay in § 4.1.

3.3.4. *Scalar overlapping different regions*

Imagine some scalar spread out over all three regions of the periodically moving vortex. After a short time, determined by the scalar variance decay in the core region, we expect a fast exponential decay in the chaotic region, which then crosses over into a slower algebraic decay in the KAM-tori region. Therefore, after a relatively short time required to rub off scalar fluctuations in the core and chaotic regions of the

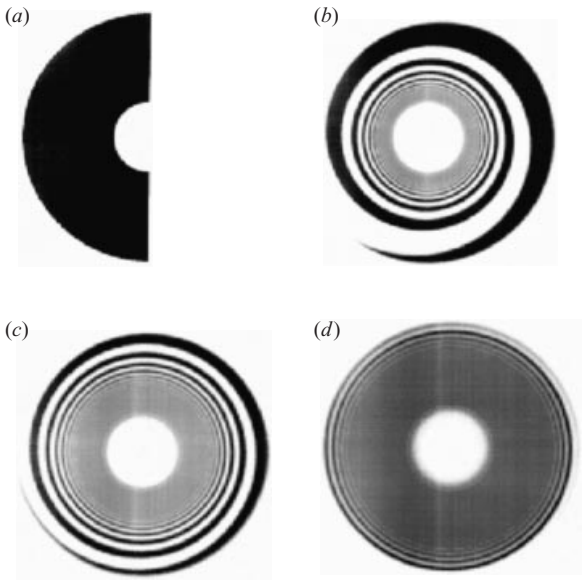

FIGURE 4. Evolution of a patch of scalar in the KAM-tori region of a sinusoidally moving vortex with $\alpha = 2$ and $\xi = 0.1$. Scalar concentration is given as grey shades with black representing maximal concentration. (*a*) Initial scalar distribution at time $t = 0$ with inner radius 1.4 and outer radius 5, (*b*) scalar field at $t = 99$, (*c*) scalar field at $t = 198$ and (*d*) scalar field at $t = 594$. Note the production of finer and finer spiral structure by the action of the vortex and the diffused core which is growing with time.

unsteady vortex, the only scalar fluctuations left are in the KAM-tori region and they determine the longer time decay of the scalar variance. In the KAM-tori region we can relate the geometrical properties of the scalar with its decay properties.

4. Simulation of advection–diffusion in the periodically moving vortex

In order to verify our predictions for the decay of the scalar variance in the chaotic region and the KAM-tori region of the periodically moving vortex, we now present and analyse results of a computer simulation of scalar advection–diffusion in a periodically moving vortex.

The advection–diffusion equation is solved numerically on a grid with either 500×500 or 800×800 points in the angular and radial directions of a polar coordinate system. The resolution is enhanced towards the centre of the vortex, because of the expected increased amount of fine structure in this region. In order to maintain sufficiently sharp gradients over a long time, as is required for large Péclet numbers, we used a second-order-accurate advection scheme proposed by Roe, see Sweby (1984). The numerical scheme is oscillation free, which is achieved by obeying the total variance diminishing condition. The diffusive fluxes are treated as source terms, again in second-order accuracy. We have periodic boundary conditions in the angular direction and homogeneous Neumann conditions in the radial direction.

4.1. *Advection–diffusion in the KAM-tori region*

In order to test our conjecture for the scalar variance decay in the KAM-tori region, we investigate the advection and diffusion in this region for different values of the exponent α of the velocity field. All simulations are carried out at the high Péclet

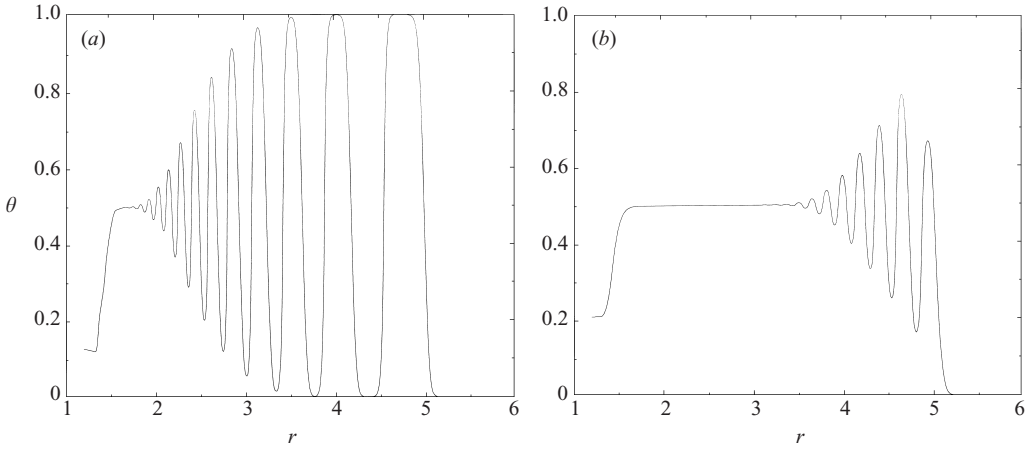

FIGURE 5. Radial cut through the scalar field advected by the velocity field of a sinusoidally moving vortex with $\xi = 0.1$ and $\alpha = \frac{1}{2}$. (*a*) $t = 37$: Spiral structure is fully developed and the inner part starts to decay because of its finer structure. (*b*) $t = 116$: The completely diffused inner core is now visible. We do not see any regions with enhanced mixing which would hint at the influence of small chaotic regions.

number of $Pe = 10^5$. Simulations with even higher Péclet numbers would have involved much higher grid resolutions and were therefore not feasible. The initial distribution of scalar is a half-ring (see figure 4*a*), filling the left part of the plane with inner radius $r_i = 1.4$ and outer radius $r_o = 5$. Note that the inner radius is larger than 1 and therefore the scalar patch lies in the KAM-tori region.

The evolution of the scalar field for $\alpha = 2$ is shown in figure 4. The series of pictures visualizes the production of finer and finer spiral scalar structure through the action of the vortex. When the spiral structure is fine enough, the diffusion finally smooths it out. The growing diffused core is a result of this smoothing out process.

In order to support the argument that chaotic regions in the KAM-tori region are irrelevant to the decay of the scalar variance, which is the basis of the freezer transformation in § 3.3.3, we also look at radial cuts through the scalar field. We have shown that the chaotic regions are larger for smaller α, and we therefore investigate radial cuts for $\alpha = \frac{1}{2}$. Figure 5 shows cuts through the scalar field at two different times. The cuts show no small regions where mixing is enhanced as we would expect in a chaotic region. We can therefore conclude that, at least in our simulation with finite resolution, the chaotic regions do not seem to have an influence on mixing in the KAM-tori region. Note that this does not necessarily mean that chaotic regions have no influence on scales which can be resolved by a simulation. One could imagine a high-resolution simulation, which would currently be very expensive, where the chaotic regions start to have an influence, even affecting scales currently resolved with our simulation.

Finally we look at our prediction of the scalar variance decay in the KAM-tori region of the periodically moving vortex. In figure 6 we compare the variance decay with the prediction (2.24) for three different values of $\alpha = \frac{1}{2}$, 1 and 2. We observe that it is rather difficult to find a region with an undisputable power law. It may be that well-defined power laws require even higher Péclet numbers. However as already pointed out at the beginning of this section, it was not feasible to go to higher Péclet numbers for computational reasons. Comparing the predictions with the simulated

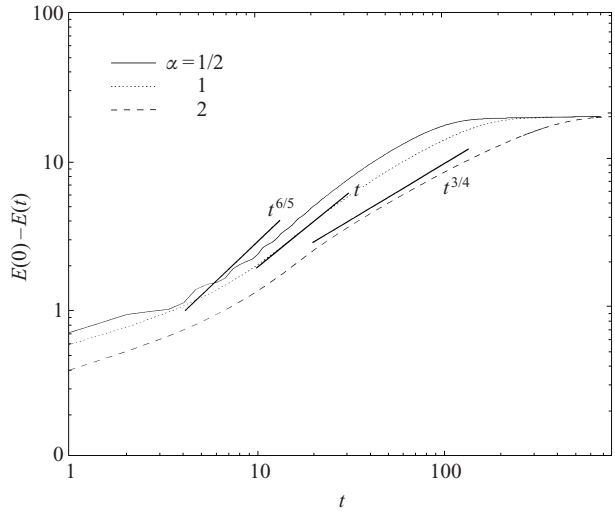

FIGURE 6. Behaviour of $E(0) - E(t)$ in the KAM-tori region of a sinusoidally moving vortex with $\xi = 0.1$ and $\alpha = \frac{1}{2}$, 1 and 2. Theoretical asymptotic scaling (2.24) is indicated by straight lines. The scalar variance decays the faster the smaller the value of α and therefore the larger the Kolmogorov capacity $D_K = 2/(1+\alpha)$. The Kolmogorov capacity can be inferred directly from a snapshot of the advected scalar field.

evolution, we find that there is at least qualitative agreement. In particular, the decay is indeed faster for smaller values of α and therefore higher values of D_K as predicted by (2.24). The agreement seems to be better for larger values of α, which is the limit where the chaotic regions become thinner.

As the variance decay does not produce very clear power laws, we also compare the growth of the diffused core with our prediction (2.14). Figure 7 shows the growth of the diffused core for $\alpha = \frac{1}{2}$ and $\alpha = 1$, extracted from cuts through the scalar field similar to the cuts in figure 5. We get clear power laws from the simulation. In comparison with the theoretical predictions, the simulated growth of the diffused core is qualitatively in agreement with the predicted growth; however we observe that the measured exponent differs from the predicted one by about 10%. As this discrepancy does not occur in the unperturbed flow, we consider it an effect of the periodic movement, which is not explained by our freezer transformation conjecture.

4.2. *Advection–diffusion in the chaotic region*

Now we investigate the decay of the scalar variance in the chaotic region of the periodically moving vortex. Looking at figure 8 and comparing it with figure 4, we see the qualitative difference between chaotic advection–diffusion and non-chaotic advection–diffusion.

Due to the exponential stretching in the chaotic region, we expect the variance decay to be exponential and therefore much faster than in the non-chaotic region. Unfortunately the size of the chaotic region in this particular periodically moving vortex is very small. Therefore we cannot convincingly show the exponential decay. However, we can clearly see that the variance decays faster in the chaotic region than it does in the non-chaotic region, see figure 9.

Furthermore we can show that the scalar aligns itself along the chaotic unstable manifold (see for example Ghosh, Leonard & Wiggins 1998). We can generate an impression of the chaotic unstable manifold by looking at the Poincaré map of the

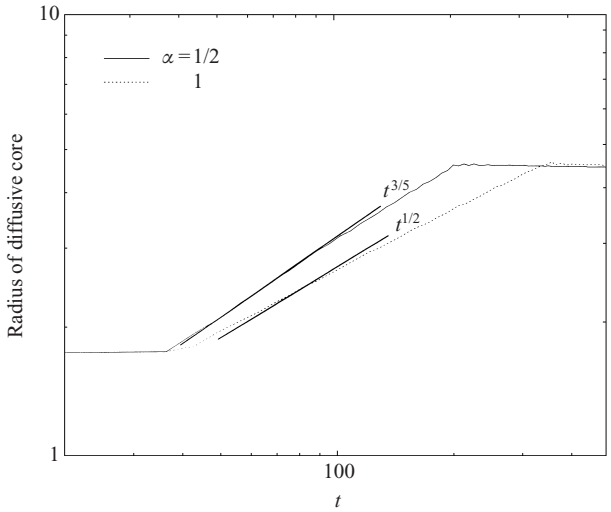

FIGURE 7. Growth of the radius of the diffused core (see figure 4) in the KAM-tori region of the sinusoidally moving vortex for $\alpha = \frac{1}{2}$ and $\xi = 0.1$. Theoretical asymptotic scaling (2.14) is indicated by a straight line. The constant radius for short times is due to a threshold setting in the algorithm used to determine the radius. The apparently constant radius for large times is the radius of the diffused core when the spiral structure has been completely rubbed off.

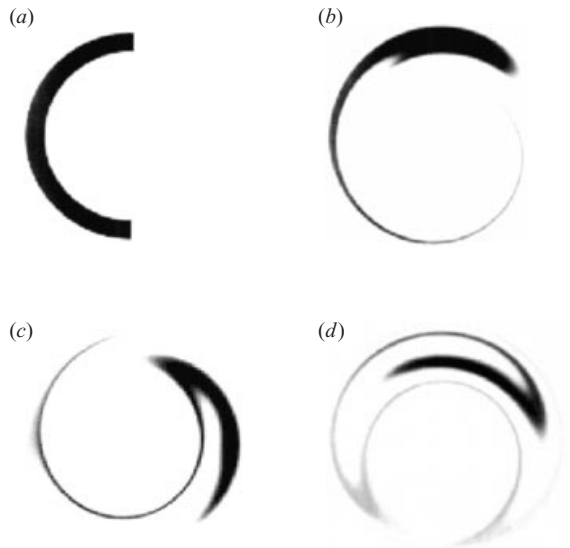

FIGURE 8. Evolution of a patch of scalar in the chaotic region of the sinusoidally moving vortex with $\alpha = 1$ and $\xi = 0.1$. Scalar concentration is given as grey shades with black representing maximal concentration. (*a*) Initial scalar distribution at time $t = 0$ with inner radius 0.9 and outer radius 1.1, (*b*) scalar field at $t = 1$, (*c*) scalar field at $t = 3.7$ and (*d*) scalar field at $t = 9$.

chaotic region in figure 10(*c*). Comparing this with images of the scalar after 7 and 8 periods of the displacement (figures 10*a* and 10*b*), we indeed find the scalar distributed along the chaotic unstable manifold. Note that during the time between images 10(*a*) and 10(*b*), the manifold performs one full rotation and hence pictures taken during this time look different from pictures at the beginning and end of the full rotation,

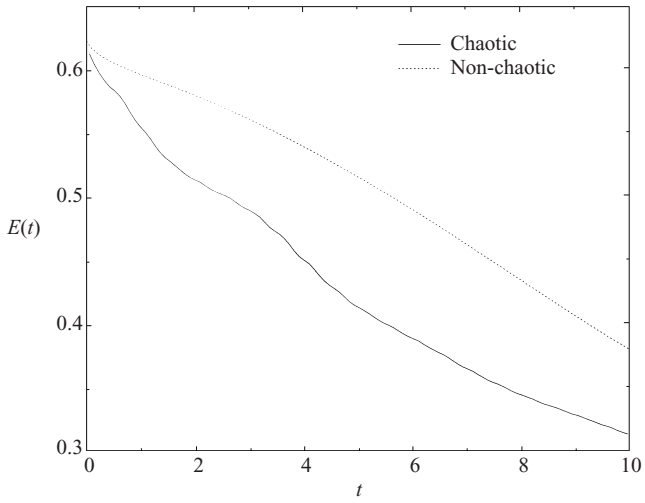

FIGURE 9. Comparison of the decay of the variance $E(t)$ in the chaotic region of a periodically moving vortex with the decay of the same scalar patch positioned at the same place with respect to the centre of vortex in the non-moving and therefore non-chaotic vortex. We see that the scalar decays faster in the chaotic region.

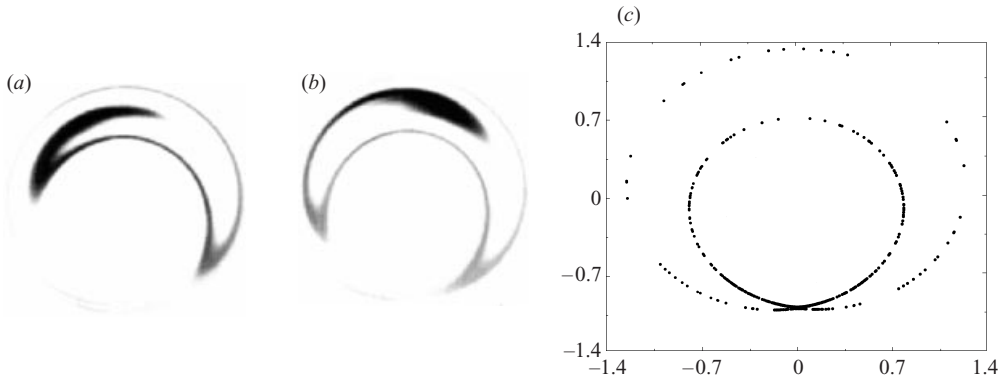

FIGURE 10. Scalar in the chaotic region of the periodically moving vortex after (*a*) 7 and (*b*) 8 periods of the displacement in comparison with a Poincaré cut (*c*) of the chaotic manifold. We see that the scalar gets attracted to the chaotic manifold and therefore similar scalar patterns reappear after a full period of the displacement.

i.e. at periods 7 and 8. This is the same process that has been observed by Rothstein, Henry & Gollup (1999), who have seen the reappearance of similar patterns in a more complicated chaotic time-periodic flow in the laboratory.

5. Summary, applications, and outlook

In this paper we have investigated passive scalar advection and diffusion in two-dimensional vortical flows. In particular we have looked at scalar variance decay in singular, frozen, non-circular symmetric vortices as well as in periodically moving singular vortices.

We have derived the asymptotic behaviour of the passive scalar field using streamline coordinates in the range of times where the scalar has developed a fine structure

which has not yet been completely rubbed off by diffusion. We have derived an asymptotic solution of the scalar field and shown that the scalar variance decays algebraically when the frequencies of nested streamlines decay algebraically as a function of their distance from the centre. The decay exponent has been calculated and is found to depend on the geometry of the streamlines and the exponent of the streamline frequencies.

For arbitrary nested streamline geometries, we have presented a method which allows in principle the streamlines and their frequencies to be reconstructed from just two snapshots of the long time advected scalar before it has been totally homogenized by diffusion. We can predict the scalar variance decay for arbitrary nested streamline geometries from just two snapshots of the advected scalar.

The periodically moving singular vortex is a model which comes closer to the kind of vortices one encounters in nature, such as the polar vortex. Our discussion has revealed that three different regions (core, chaotic and KAM-tori) exist in this vortex. In addition to the fast exponential decay in the chaotic region (Pierrehumbert 1994; Toussaint *et al.* 1995; Antonsen *et al.* 1996), we have shown that the variance decays much more slowly in the outer KAM-tori region and that this decay is slower for smaller Kolmogorov capacities of the scalar field. We have developed a quantitative prediction of the scalar advection and diffusion in the KAM-tori region which is based on a transformation from a time-periodic problem to a frozen advection problem. The assumptions on which the transformation is based were checked against a simulation.

This paper contributes to the study of the connections between variance decay and geometry (Angilella & Vassilicos 1998; Flohr & Vassilicos 1997). The quantification of the variance decay by means of a purely geometrical quantity could have wide applications, for example in atmospheric sciences. One could imagine, at least in principle, taking satellite images of an advected passive tracer in an atmospheric vortex, for example the polar vortex, and determining properties of the vortex (such as the period of its streamlines) which could be used to predict the nature and time scale of scalar mixing in the vortex. This work is a first step towards such a widely applicable diagnostic and predictive tool.

Future research might comprise the generalization of the present work to an aperiodic, randomly moving vortex. Another interesting generalization lies in the study of the evolution of reacting chemicals in flows similar to the ones studied in this work. The methods developed here could be generalized in order to relate chemical reactions to their spatial distribution.

We thank P. Flohr for contributing his original advection–diffusion code and one of the referees for valuable comments. A. W. and J. C. V. gratefully acknowledge support by the Dr Karl Wamsler Foundation, NERC and the Royal Society.

Appendix A. Characteristic of the pure advection equation

In order to find the characteristic $\varphi_0(\rho, \varphi, t)$ (2.10), we first derive the solution $\varphi(\rho, \varphi_0, t)$ to the advection equation

$$\frac{\partial}{\partial t}\varphi(\rho, t) = \Omega(\rho, \varphi). \tag{A 1}$$

Then we invert $\varphi = \varphi(\rho, \varphi_0, t)$ and get $\varphi_0 = \varphi_0(\rho, \varphi, t)$.

Due to the 2π-periodicity of φ, there exists a period $T(\rho)$, which fulfils

$$\varphi(\rho, \varphi_0, t + T(\rho)) = \varphi(\rho, \varphi_0, t) + 2\pi. \tag{A 2}$$

Therefore we can write the solution of the advection equation (A 1) in the form

$$\varphi(\rho, \varphi_0, t) = \bar{\Omega}(\rho)t + \xi(\rho, \varphi_0, t), \tag{A 3}$$

where

$$\bar{\Omega}(\rho) := \frac{2\pi}{T(\rho)} \tag{A 4}$$

and $\xi(\rho, \varphi_0, t)$ is $T(\rho)$-periodic in t. It is convenient to describe the initial condition φ_0 in terms of a time shift t_0:

$$\varphi(\rho, \varphi_0, t) = \bar{\Omega}(\rho)(t + t_0) + \xi(\rho, 0, t + t_0), \tag{A 5}$$

where

$$\varphi_0 = \overline{\Omega}(\rho)t_0 + \xi(\rho, 0, t_0). \tag{A 6}$$

Because Ω in (A 1) is strictly positive, the solution $\varphi(\rho, \varphi_0, t)$ is strictly monotonic in time and we can therefore solve (A 5) for $t + t_0$:

$$t + t_0 = \frac{\varphi}{\bar{\Omega}(\rho)} + \eta(\rho, \varphi), \tag{A 7}$$

where the function η is 2π-periodic in φ. Inserting (A 7) in (A 6) yields φ_0 as a function of ρ, φ and t:

$$\begin{aligned}\varphi_0(\rho, \varphi, t) &= \bar{\Omega}(\rho)\left(\frac{\varphi}{\bar{\Omega}(\rho)} + \eta(\rho, \varphi) - t\right) + \xi\left(\rho, 0, \frac{\varphi}{\bar{\Omega}(\rho)} + \eta(\rho, \varphi) - t\right) \\ &= \varphi - \bar{\Omega}(\rho)t + \bar{\Omega}(\rho)\eta(\rho, \varphi) + \xi\left(\rho, 0, \frac{\varphi}{\bar{\Omega}(\rho)} + \eta(\rho, \varphi) - t\right) \\ &=: \varphi - \bar{\Omega}(\rho)t + \zeta(\rho, \varphi, t).\end{aligned} \tag{A 8}$$

It is now easy to check that $\zeta(\rho, \varphi, t)$ is 2π-periodic in φ and $T(\rho)$-periodic in t.

Appendix B. Asymptotic solution for scalar advection–diffusion in arbitrary nested streamline coordinates

In this appendix, we derive the asymptotic solution to (2.7) in the range of times $1 \ll t \ll Pe^{1/3}$. The left-hand side of (2.7), i.e. the advective contribution, reads, together with (2.11),

$$\frac{\partial}{\partial t}\Theta(\rho, \varphi, t) + \Omega(\rho, \varphi)\frac{\partial}{\partial \varphi}\Theta(\rho, \varphi, t) = \sum_n \mathrm{e}^{\mathrm{i}n(\varphi - \bar{\Omega}(\rho)t + \zeta(\rho, \varphi, t))}\frac{\partial}{\partial t}\Theta_n(\rho, t). \tag{B 1}$$

The right-hand side, i.e. the diffusive contribution, of (2.7) can also be expressed in orthogonal streamline coordinates. Expressing the Laplacian in streamline coordinates, we find

$$\begin{aligned}\nabla^2\Theta &= \frac{1}{g_\rho g_\varphi}\left[\frac{\partial}{\partial \rho}\left(\frac{g_\varphi}{g_\rho}\frac{\partial}{\partial \rho}\right) + \frac{\partial}{\partial \varphi}\left(\frac{g_\rho}{g_\varphi}\frac{\partial}{\partial \varphi}\right)\right]\Theta \\ &= \underbrace{\frac{1}{g_\rho^2}\frac{\partial^2}{\partial \rho^2}\Theta}_{\text{(i)}} + \underbrace{\frac{1}{g_\rho g_\varphi}\left(\frac{\partial}{\partial \rho}\frac{g_\varphi}{g_\rho}\right)\frac{\partial}{\partial \rho}\Theta}_{\text{(ii)}} + \underbrace{\frac{1}{g_\varphi^2}\frac{\partial^2}{\partial \varphi^2}\Theta}_{\text{(iii)}} + \underbrace{\frac{1}{g_\rho g_\varphi}\left(\frac{\partial}{\partial \varphi}\frac{g_\rho}{g_\varphi}\right)\frac{\partial}{\partial \varphi}\Theta}_{\text{(iv)}}.\end{aligned} \tag{B 2}$$

Inserting (2.11) to calculate term (i) we get

$$\frac{1}{g_\rho^2}\frac{\partial^2}{\partial\rho^2}\Theta = \frac{1}{g_\rho^2}\sum_n \mathrm{e}^{\mathrm{i}n(\varphi-\bar{\Omega}(\rho)t+\zeta(\rho,\varphi,t))}\left[\underbrace{-n^2t^2\,(\bar{\Omega}'(\rho))^2\,\Theta_n}_{(*)} + O(t)\Theta_n\right]. \tag{B 3}$$

Terms (ii) to (iv) give contributions of the following orders:

$$\text{(ii)} = \sum_n \mathrm{e}^{\mathrm{i}n(\varphi-\bar{\Omega}(\rho)t+\zeta(\rho,\varphi,t))}O(t)\Theta_n(\rho,t), \tag{B 4a}$$

$$\text{(iii)} = \sum_n \mathrm{e}^{\mathrm{i}n(\varphi-\bar{\Omega}(\rho)t+\zeta(\rho,\varphi,t))}O(1)\Theta_n(\rho,t), \tag{B 4b}$$

$$\text{(iv)} = \sum_n \mathrm{e}^{\mathrm{i}n(\varphi-\bar{\Omega}(\rho)t+\zeta(\rho,\varphi,t))}O(1)\Theta_n(\rho,t). \tag{B 4c}$$

The $O(t)$ and $O(1)$ symbols in equations (B 3) and (B 4) also contain functions periodic in t stemming from $\zeta(\rho,\varphi,t)$ and its derivatives as well as $\partial/\partial\rho$ derivatives acting on Θ_n. Note that the evolution of $\Theta_0(\rho,t)$ is governed by (B 3) and (B 4*a*). An explicit analysis shows that $\Theta_0(\rho,t)$ varies only on time scales $O(Pe)$. Therefore it can be regarded as time independent in the range of times under consideration here, $O(Pe^{1/3}) \ll O(Pe)$. Hence in the limit $1 \ll t \ll Pe^{1/3}$ when the vortex has produced a lot of fine structure, which has not yet completely decayed, i.e. $\Theta_{n\neq 0} \neq 0$, the leading-order contribution is (*) in (B 3).

The advection–diffusion equation (2.7) therefore reads, in the long time limit $t \gg 1$ (taking into account the results (B 1) and (B 3)),

$$\sum_n \mathrm{e}^{\mathrm{i}n(\varphi-\overline{\Omega}(\rho)t+\zeta(\rho,\varphi,t))}\frac{\partial}{\partial t}\Theta_n(\rho,t) \approx -\frac{1}{g_\rho^2(\rho,\varphi)}\sum_n \mathrm{e}^{\mathrm{i}n(\varphi-\overline{\Omega}(\rho)t+\zeta(\rho,\varphi,t))}\,Pe^{-1}\,n^2(\overline{\Omega}'(\rho))^2\,t^2\,\Theta_n(\rho,t). \tag{B 5}$$

In order to find an equation for each scalar field component, we have to find the convolution of the metrical factor $1/g_\rho^2$ with the scalar field. This can be achieved by Fourier transforming the metric pre-factor with characteristic coordinates (A 5)

$$f_n(\rho,t) = \frac{1}{2\pi}\int_0^{2\pi}\mathrm{d}\varphi\,\frac{1}{g_\rho^2(\rho,\varphi)}\,\mathrm{e}^{-\mathrm{i}n(\varphi-\bar{\Omega}(\rho)t+\zeta(\rho,\varphi,t))}. \tag{B 6}$$

It is important for what follows to note that $f_0 = 1$. This follows immediately from our choice (2.4) for the ρ-parameterization. All other f_n are bound, i.e. $|f_n| \leqslant 1$ and $T(\rho)$-periodic in t. These properties follow immediately from $|\int f| \leqslant \int |f|$ and (A 4), (2.10), respectively. Writing the convolution of two Fourier series as

$$A_n * B_n := \sum_{m=-\infty}^{\infty} A_m B_{n-m}, \tag{B 7}$$

we find for the Θ_n in (B 5)

$$\frac{\partial}{\partial t}\Theta_n(\rho,t) = -(f_n(\rho,t)) * \left(Pe^{-1}\,n^2(\bar{\Omega}'(\rho))^2\,t^2\,\Theta_n(\rho,t)\right) = -\sum_m \underbrace{Pe^{-1}f_{n-m}(\rho,t)m^2(\bar{\Omega}'(\rho))^2\,t^2}_{M_{nm}:=}\,\Theta_m. \tag{B 8}$$

This is a first-order linear differential equation for the vector $\boldsymbol{\Theta} = (\{\Theta_n\})$ with a given coefficient matrix $\boldsymbol{M} = (\{M_{nm}\})$

$$\frac{\partial}{\partial t}\boldsymbol{\Theta}(\rho, t) = -\boldsymbol{M}(\rho, t)\,\boldsymbol{\Theta}(\rho, t). \tag{B 9}$$

Its solution can be written as

$$\boldsymbol{\Theta}(\rho, t) = \underbrace{\exp\left(-\int_0^t \mathrm{d}t'\,\boldsymbol{M}(\rho, t')\right)}_{=:\boldsymbol{S}(\rho,t)}\boldsymbol{\Theta}(\rho, t=0). \tag{B 10}$$

We can split the solution matrix $\boldsymbol{S}$ into one matrix which contains diagonal elements and another which contains all non-diagonal elements:

$$\boldsymbol{S} = \exp(-\boldsymbol{A})\exp(-\boldsymbol{B}) = \begin{pmatrix} \mathrm{e}^{-A_{11}} & & 0 \\ & \ddots & \\ 0 & & \mathrm{e}^{-A_{nn}} \end{pmatrix}\exp(-\boldsymbol{B}). \tag{B 11}$$

The diagonal elements ($m = n$) are given by

$$A_{nn} \equiv \int_0^t \mathrm{d}t'\,M_{nn} = \frac{Pe^{-1}}{3}n^2(\bar{\Omega}'(\rho))^2\,t^3 = O\left(\frac{t^3}{Pe}\right) \tag{B 12}$$

and $A_{n\neq m} := 0$. However, all non-diagonal elements ($m \neq n$) are given by

$$B_{n\neq m} \equiv \int_0^t \mathrm{d}t'\,M_{n\neq m} = \int_0^t \mathrm{d}t'\,Pe^{-1}f_{n-m}(\rho, t')m^2(\bar{\Omega}'(\rho))^2\,t'^2 = O\left(\frac{t^2}{Pe}\right) \tag{B 13}$$

and $B_{nn} = 0$. The non-diagonal elements are $O(t^2/Pe)$ in the long time limit $t \gg 1$, because f_n is $T(\rho)$-periodic. Now we can identify two time ranges for the solution matrix. For $(\bar{\Omega}'(\rho))^2\,t^3/Pe \gg 1$ (neglecting the influence of n^2) the matrix $\exp(-\boldsymbol{A})$ vanishes and therefore $\boldsymbol{S}$ vanishes, too. However for $(\bar{\Omega}'(\rho))^2\,t^3/Pe \leqslant 1$, the non-diagonal elements of B_{nm} are of $O(1/t)$, and we can write $\exp(-\boldsymbol{B}) = 1 - O(1/t)$. Hence the time-evolution of Θ_n in the time range $t \gg 1$ and $(\Omega'(\rho))^2\,t^3/Pe \leqslant 1$ is given by

$$\Theta_n(\rho, t) = \sum_m \left[\exp\left(-\tfrac{1}{3}n^2(\bar{\Omega}'(\rho))^2\frac{t^3}{Pe}\right)\delta_{nm} - \left[O\left(\frac{1}{t}\right)\right]_{n\neq m}\right]\Theta_m(\rho, t=0). \tag{B 14}$$

For $(\Omega'(\rho))^2\,t^3/Pe \gg 1$, Θ_n asymptotically vanishes. Thus the solution of the advection–diffusion equation for a nested, closed streamline geometry reads, to leading order,

$$\Theta_n(\rho, t) = \exp\left(-\tfrac{1}{3}n^2(\bar{\Omega}'(\rho))^2\frac{t^3}{Pe}\right)\Theta_n(\rho, t=0) \tag{B 15}$$

in the time range $1 \ll t \ll Pe^{1/3}$.

Appendix C. Elliptical streamline coordinates

To illustrate the role of μ, we can for example examine the leading contribution of $a_0(\rho)$ in the case of elliptical coordinates. Elliptical coordinates can be defined by mapping the coordinates (ρ, φ) onto Cartesian coordinates $\boldsymbol{x} = (x, y)$

$$x = c\cosh(r(\rho))\cos(\varphi), \quad y = c\sinh(r(\rho))\sin(\varphi), \tag{C 1a,b}$$

where c is a parameter of the coordinate system equal to half the distance between the focus points of the ellipses. The function $r(\rho)$ is chosen such that condition (2.4) is fulfilled. For $\rho \ll 1$ we can then calculate the metric components of this coordinate system using $g_\rho = |(\partial/\partial\rho)\boldsymbol{x}|$ and $g_\varphi = |(\partial/\partial\varphi)\boldsymbol{x}|$:

$$g_\rho(\rho,\varphi) = c\left(\frac{4\pi}{3\rho}\right)^{1/3}\sqrt{(2\pi)^{2/3}\left(\tfrac{3}{2}\rho\right)^{4/3}+\sin^2(\varphi)}, \tag{C 2a}$$

$$g_\varphi(\rho,\varphi) = c\sqrt{(2\pi)^{2/3}\left(\tfrac{3}{2}\rho\right)^{4/3}+\sin^2(\varphi)}. \tag{C 2b}$$

Using (2.17) we can now calculate $a_0(\rho)$ to leading order in $\rho \ll 1$ and find

$$a_0(\rho) = c^2(12\rho)^{-1/3}. \tag{C 3}$$

Hence, for elliptical coordinates close to the origin ($\rho \ll 1$), $\mu = -\frac{4}{3}$. The elliptical coordinates are therefore an example of streamline coordinates with non-zero μ.

Appendix D. Leading contribution to the variance decay

In this appendix, we derive the leading contribution to the decay of the scalar variance $E(0) - E(t)$. The term $\exp(\mathrm{i}(n+m)(\varphi - \bar{\Omega}(\rho)t + \zeta(\rho,\varphi,t)))$ in (2.16) leads to a time-dependent coupling between the Fourier modes Θ_n and Θ_m. This time-dependent coupling may lead to oscillations in the decay. However we show in the following that these oscillations happen on a much smaller time scale than the overall decay and therefore do not affect the general character of the decay. For a given ρ, the coupling term is $T(\rho)$-periodic. Therefore its time dependence varies on a scale $t < 1$. In contrast, the term $\exp(-(n^2+m^2)(\bar{\Omega}'(\rho))^2(t+\tau)^3/(3Pe))$ in (2.16) varies considerably only on scales $t \gg 1$. Assume the argument of the exponential to be small, i.e. $(n^2+m^2)(\bar{\Omega}'(\rho))^2 t^3/(3Pe) \ll 1$, then the variation of the exponential on a time scale of order 1 is small:

$$\exp\left(-(n^2+m^2)(\bar{\Omega}'(\rho))^2\frac{(t+1)^3}{3Pe}\right) - \exp\left(-(n^2+m^2)(\bar{\Omega}'(\rho))^2\frac{t^3}{3Pe}\right) = O\left(\frac{1}{t}\right). \tag{D 1}$$

For large arguments, i.e. $(n^2+m^2)(\bar{\Omega}'(\rho))^2 t^3/(3Pe) \gg 1$, the exponential vanishes and hence its variation on a time scale of order 1 is again small. Therefore the short time scale variations induced by the coupling term can be neglected when we are interested in the general decay behaviour in the range of times $1 \ll t \ll Pe^{1/3}$.

In the limit $\rho \to 0$, $a_0(\rho)$ has a leading contribution to the product of the metrical components. Hence the leading order of the energy decay is obtained by replacing the product of the geometrical factors g_ρ and g_φ with a_0. Therefore the leading behaviour of (2.16) can be inferred from

$$E(t) \propto \int \mathrm{d}\rho\, a_0(\rho)\exp\left(-(n^2+m^2)(\bar{\Omega}'(\rho))^2\frac{t^3}{3Pe}\right). \tag{D 2}$$

Transforming the integration variable in (D 2) to $x = (\bar{\Omega}'(\rho))^2 t^3/(3Pe)$, we obtain, together with (2.19), the power law

$$E(0) - E(t) \propto \left(\frac{t^3}{Pe}\right)^{\frac{2+\mu}{2}\frac{\beta}{1+\beta}} \tag{D 3}$$

for the decay of the scalar variance. The result is valid in the vicinity of the streamline algebraic singularity in a range of times $1 \ll t \ll Pe^{1/3}$.

In (D 2) we have neglected the ρ dependence of the scalar field Θ. As long as Θ does not possess a significant power law, its ρ dependence does not change the scaling exponent of the variance decay. For a constant-concentration scalar field, power laws can only occur at the boundary of the patch and therefore only affect the very short or very long time behaviour of the decay. If the field has a known power law in ρ, it is possible to calculate the corrected decay exponent of its variance by inserting the ρ-dependent field in (2.21) and carrying out the integral.

REFERENCES

Angilella, J. & Vassilicos, J. 1998 Spectral, diffusive and convective properties of fractal and spiral fields. *Physica* D **124**, 23.

Antonsen, T., Fan, Z., Ott, E. & Garcia-Lopez, E. 1996 The role of chaotic orbits in the determination of power spectra of passive scalars. *Phys. Fluids* **8**, 3094–3104.

Aref, H. 1984 Stirring by chaotic advection. *J. Fluid Mech.* **143**, 1–21.

Arnold, V. (Ed.) 1988 *Dynamical Systems III*. Springer.

Batchelor, G. 1956 On steady laminar flow with closed streamlines at large Reynolds numbers. *J. Fluid Mech.* **1**, 177–190.

Batchelor, G. 1967 *An Introduction to Fluid Dynamics*. Cambridge University Press.

Birkhoff, G. 1935 Nouvelles recherches sur les systèmes dynamiques. *Pont. Acad. Sci. Novi Lyncaei* **1**, 85.

Corrsin, S. 1951 On the spectrum of isotropic temperature fluctuations in an isotropic turbulence. *J. Appl. Phys.* **22**, 469–473.

Dritschel, D. 1998 On the persistence of non-axisymmetric vortices in inviscid two-dimensional flows. *J. Fluid Mech.* **371**, 141–155.

Flohr, P. & Vassilicos, J. 1997 Accelerated scalar dissipation in a vortex. *J. Fluid Mech.* **348**, 295.

Frisch, U. 1995 *Turbulence*. Cambridge University Press.

Ghosh, A., Leonard, A. & Wiggins, S. 1998 Diffusion of a passive scalar from a no-slip boundary into a two-dimensional chaotic advection field. *J. Fluid Mech.* **372**, 119–163.

Hunt, J. & Vassilicos, J. 1991 Kolmogorov's contribution to the physical and geometrical understanding of small-scale turbulence and recent developments. *Proc. R. Soc. Lond.* A **434**, 183–210.

Le Dizès, S. 2000 Non-axisymmetric vortices in two dimensional flows. *J. Fluid Mech.* **406**, 175–198.

McIntyre, M. 1989 On the antarctic ozone hole. *J. Atmos. Terr. Phys.* **51**, 29–43.

Oboukhov, A. 1949 Structure of the temperature field in a turbulent flow. *Izv. Acad. Nauk SSSR, Geogr. Geofiz* **13**, 58–69.

Ottino, J. 1989 *The Kinematics of Mixing: Stretching, Chaos, and Transport*. Cambridge University Press.

Pierrehumbert, R. 1994 Tracer microstructure in the large-eddy dominated regime. *Chaos, Solitons & Fractals* **4**, 1091–1110.

Rhines, P. & Young, W. 1983 How rapidly is passive scalar mixed within closed streamlines. *J. Fluid Mech.* **133**, 133–145.

Rossi, L., Lingevitch, J. & Bernoff, A. 1997 Quasi-steady monopole and tripole attractors for relaxing vortices. *Phys. Fluids* **9**, 2329–2338.

Rothstein, D., Henry, E. & Gollup, J. 1999 Persistent patterns in transient chaotic fluid mixing. *Nature* **401**, 770–772.

Sweby, P. 1984 High resolution schemes using flux limiters for hyperbolic conservation laws. *SIAM J. Numer. Anal.* **21**, 995–1011.

Tang, X. & Boozer, A. 1999 A lagrangian analysis of advection–diffusion equation for a three dimensional chaotic flow. *Phys. Fluids* **11**, 1418–1434.

Toussaint, V., Carrière, P. & Raynal, F. 1995 A numerical eulerian approach to mixing by chaotic advection. *Phys. Fluids* **7**, 2587–2600.

VASSILICOS, J. & BRASSEUR, J. 1996 Self-similar spiral flow structure in low Reynolds number isotropic and decaying turbulence. *Phys. Rev.* E **54**, 467–485.

VASSILICOS, J. & FUNG, J. 1995 The self similar topology of passive interfaces advected by two-dimensional turbulent-like flows. *Phys. Fluids* **7**, 1970–1998.

VASSILICOS, J. & HUNT, J. 1991 Fractal dimensions and spectra of interfaces with application to turbulence. *Proc. R. Soc. Lond.* A **435**, 505–534.